Journal of Information Hiding and Multimedia Signal Processing ©2015 ISSN 2073-4212
Ubiquitous International Volume **6**, Number **3**, May **2015**

A Novel Explicit Multi-focus Image Fusion Method

Kun Zhan, Jicai Teng, Qiaoqiao Li and Jinhui Shi

School of Information Science and Engineering
Lanzhou University
Gausu, 730000,China
kzhan@lzu.edu.cn; tengjc13@lzu.edu.cn; liqq13@lzu.edu.cn; shijh14@lzu.edu.cn

Received November, 2014; revised February, 2015

Abstract. We propose a multi-focus image fusion method. The energy of Laplacian of input images is obtained to decide which portions of the input images are in better focus, and the majority filter offers a means of spreading the focused regions to neighborhood. The edge-preserving guided image filter is applied to reduce the block effect. We conduct several experiments which demonstrate that it provided a better performance than the state of the art fusion methods in visual and quantitative evaluations.
Keywords: Image fusion, Multi-focus, Energy of laplacian, Majority filter, Guided filter.

1. **Introduction.** Optical lenses are widely mounted in imaging devices. A lens with long focal lengths suffers from the problem of limited depth of field, and only few objects with the depth of field are focused and others are blurred. Besides solutions making use of specialized optics [1, 2, 3] and computational imaging [4, 5], the multi-focus fusion process is highly desirable to create a single image where all objects are in focus.

Focused regions have higher frequency components than de-focused regions, and the sharp and local changes in intensity are indicated by the high frequency subbands coefficients. Multi-scale transforms are generally used for image fusion to estimate image sharpness in transform domain and select informative high frequency coefficients. Multi-scale transform incorporates and unifies techniques including subband coding, quadrature mirror filtering and pyramidal image decomposition. Burt *et al.* firstly used Laplacian pyramid for image fusion [6], later Toet *et al.* used contrast pyramid [7] and Rockinger fused image via a shift-invariant wavelet [8]. After these work more and more multi-scale methods are reported [9, 10, 11, 12], such as log-Gabor wavelet transform [13], nonsubsampled contourlet transform [14], and multi-scale weighed gradient-based method [15]. However, multi-scale methods are generally shift variant because of an underlying downsampling process, they have a high computational complexity, and the original intensity is not preserved in the fused image.

In spatial domain, the sharp and local changes in the input intensity images are directly computed from pixels or blocks [16, 17, 18]. Because the focus measures are obtained in different way, the fusion methods of spatial domain are mainly categorized into two groups: pixel-based methods [19, 20, 21] and block-based methods [22, 23, 24, 25]. The main advantages of these methods are easy to be implemented to obtain the focus measure with a low computational complexity and the output contains original focused regions from input images. However, the existing fusion schemes of spatial domain are complex,

such as methods based on artificial neural network [24, 25, 19], support vector machine [23], and image matting technique [26].

In this paper, an efficient image fusion algorithm using guided filter is proposed. The proposed image fusion scheme is compared with the state of the art methods, such as methods based on image matting technique [26], two-scale decomposition using the guided filter [27], and multi-scale weighted gradient [15], and it is also compared with the classic methods: contrast pyramid [7] and shift-invariant wavelet [8]. The comparisons indicate the efficiency of the proposed fusion scheme using three performance measures.

2. **The focus measure.** Since the quality of focus affects detecting the sharp and local changes in intensity, it is suggested to use the sum-modified Laplacian and the energy of Laplacian (EOL) for computing the focus quality [17]. Because EOL is a lower time-consuming process than the sum-modified Laplacian, we use EOL as the focus measure. EOL naturally increases with correct image focus, and each input pixels can thereby be selected until the maximum EOL is detected. EOL detection is significant for image fusion technique.

We define the second-order derivative of $f(x)$ as the difference,

$$\frac{\partial^2 f}{\partial x^2} = f(x+1) + f(x-1) - 2f(x) \tag{1}$$

The Laplacian is given by the sum of second partial derivatives of an image $I(x,y)$ of two variables with respect to each independent variable,

$$\begin{aligned} \nabla^2 I(x,y) &= \frac{\partial^2 I(x,y)}{\partial x^2} + \frac{\partial^2 I(x,y)}{\partial y^2} \\ &= I(x+1,y) + I(x-1,y) + \\ &\quad I(x,y+1) + I(x,y-1) - 4I(x,y) \end{aligned} \tag{2}$$

This equation can be implemented using the filter mask as,

$$L_1 = \begin{bmatrix} 0 & 1 & 0 \\ 1 & -4 & 1 \\ 0 & 1 & 0 \end{bmatrix}$$

The diagonal directions can be incorporated in the definition of Laplacian. We take linear combination of four directions and the formula below produces a symmetric filter mask,

$$\begin{aligned} L &= \frac{1-\alpha}{1+\alpha} \begin{bmatrix} 0 & 1 & 0 \\ 1 & -4 & 1 \\ 0 & 1 & 0 \end{bmatrix} + \frac{\alpha}{1+\alpha} \begin{bmatrix} 1 & 0 & 1 \\ 0 & -4 & 0 \\ 1 & 0 & 1 \end{bmatrix} \\ &= \frac{4}{1+\alpha} \begin{bmatrix} \frac{\alpha}{4} & \frac{1-\alpha}{4} & \frac{\alpha}{4} \\ \frac{1-\alpha}{4} & -1 & \frac{1-\alpha}{4} \\ \frac{\alpha}{4} & \frac{1-\alpha}{4} & \frac{\alpha}{4} \end{bmatrix} \end{aligned} \tag{3}$$

where α is a proportion coefficient.

The EOL focus measure of I^A and I^B is computed by,

$$M_p = (I * L)^2 \tag{4}$$

where $*$ denotes the convolution, I is an input image, L is the Laplacian operator and M_p is EOL for each pixel.

(a) (b)

FIGURE 1. An example of the majority filter, (a) the input decision map D, (b) the filtered decision map D_b.

3. **The majority filter.** As shown in Fig.1, the majority filter is applied to ensure the pixels with larger focus measures influence the decision of their neighbors more [28].

We assume that there are two input images, and they are denoted by I^A and I^B. If the center pixel comes from image I^A while the majority of the surrounding pixels come form image I^B, the center pixel value is switched to that of image I^B. The majority filter is utilized in window-based consistency verification and is given by,

$$D_b = \begin{cases} 1, & \text{if } D * W_l > \frac{l^2}{2} \\ 0, & \text{otherwise} \end{cases} \tag{5}$$

where D is the input decision map, D_b is the filtered decision map, and W_l is a sliding $l \times l$ matrix in which all values are set to 1.

The term $\frac{l^2}{2}$ can be obtained by the term $0.5 * W_l$, so the majority filter can be implemented in Algorithm 1.

Algorithm 1 The majority filter

```
D = D − 0.5;
D = D ∗ W_l
if D > 0 then
    D_b = 1
else
    D_b = 0
end if
```

4. **The guided filter.** The guided filter is a local linear model between the guidance image I and the output q [29]. It is assumed that q is a linear transform of I in a window ω_k centered at pixel k,

$$q_i = a_k I_i + b_k \ \forall i \in \omega_k \tag{6}$$

where (a_k, b_k) are the linear coefficients assumed to be constant in ω_k, and ω_k is a square window of a radius r.

The guided filter is an edge-preserving process, and q has an edge only if I has an edge because $\nabla q = a \nabla I$. The solution to (6) minimizes the difference between q and p. Specifically, the linear coefficients (a_k, b_k) are determined by minimizing the following cost function in the window,

$$E(a_k, b_k) = \sum_{i \in \omega_k} ((a_k I_i + b_k - p_i)^2 + \epsilon a_k^2) \tag{7}$$

where ϵ is a regularization parameter preventing a_k from being too large.

The coefficients a_k and b_k is solved by linear regression [30]:

$$a_k = \frac{\frac{1}{|\omega|}\sum_{i\in\omega_k}(I_i p_i - \mu_k \overline{p}_k)}{\sigma_k^2 + \epsilon} \tag{8}$$

$$b_k = \overline{p}_k - a_k \mu_k \tag{9}$$

where μ_k and σ_k^2 are the mean and variance of I in ω_k respectively, $|\omega|$ is the number of pixels in ω_k, and $\overline{p}_k$ is the mean of p in ω_k.

It can be seen from (6) that a pixel i is involved in all the windows ω_k that contain i, so the value of q_i is not identical when it is computed in different overlapping windows. In [29], all the possible values of coefficients a_k and b_k are first averaged. Then, the filtering output is estimated as follows:

$$q_i = \overline{a}_i I_i + \overline{b}_i \tag{10}$$

where $\overline{a}_i = \frac{1}{|\omega|}\sum_{k\in\omega_i} a_k$, $\overline{b}_i = \frac{1}{|\omega|}\sum_{k\in\omega_i} b_k$.

Fig.2 is an example of the guided image filter. The output q preserves the edge of the guidance image I and the filtering input p is smoothed.

(a) (b) (c)

FIGURE 2. An example of the guided filter, r=60, $\epsilon = 0.01^2$ (a) the guidance image I, (b) the filtering input p, (c) the filtered output q.

5. **The image fusion scheme.** Fig.3 is the schematic diagram for the multi-focus image fusion method.

The grayscale intensity of I^A and I^B is normalized to lie within the range [0, 1].

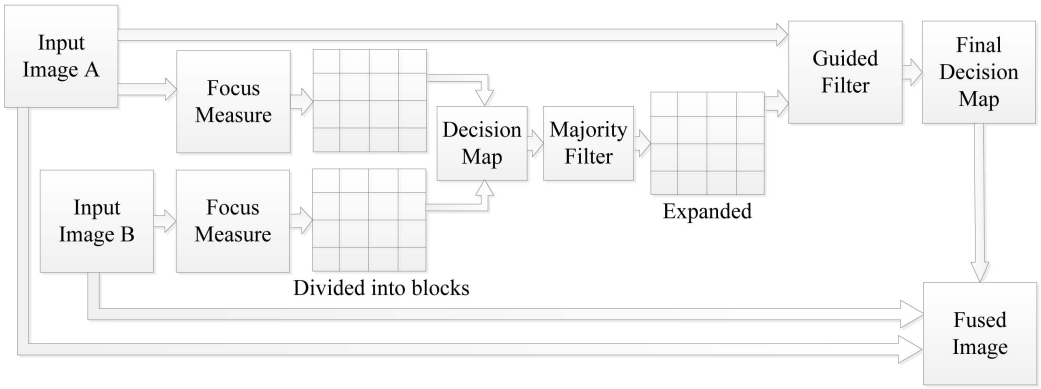

FIGURE 3. Schematic diagram for the proposed multi-focus image fusion.

The EOL focus measure of the input images are computed to obtain M_p by (4) respectively.

EOL, the matrix M_p, is divided into non-overlapping 8×8 blocks and the blocks are processed independently. The focus measure of each block is the sum of the values in the block,

$$M_b(m,n) = \sum M_p(x,y) \tag{11}$$

where x and y are pixel indexes, m and n are block indexes, and $M_b(m,n)$ is the focus measure for each block.

The focus measures in the matrix M_b are compared to obtain a binary decision map by,

$$D(m,n) = \begin{cases} 1, & \text{if } M_b^A(m,n) > M_b^B(m,n) \\ 0, & \text{otherwise} \end{cases} \tag{12}$$

where M_b^A is the focus measure for the image I^A, and M_b^B is the focus measure for the image I^B.

The focused image areas produce larger EOL metrics, and the de-focused areas produce smaller EOL metrics. So value 1 implies that a block in I^A focused while 0 implies that a block in I^B focused.

We modify the majority filter as shown in Algorithm 2, and the decision map D is filtered twice to obtain D_b by the modified majority filter.

The decision map D_b is expanded to D_p by,

$$D_p = D_b \circledast W_8 \tag{13}$$

where $\circledast$ denotes the Kronecker product, and W_8 is an 8×8 matrix in which every value is 1.

It can be seen from Fig.2 that the fused result under the decision map D_p has block effect and lose edge and texture information from input images, so the guided image filter is applied to optimize the decision map. We set the image I^A and the decision map D_p to the guidance image and the filtering image of the guided image filter respectively, and the filtered result is denoted by D_2. Therefore, the fused image is obtained from original input images using decision map D_2,

$$F(x,y) = D_2(x,y)I^A(x,y) + (1 - D_2(x,y))I^B(x,y) \tag{14}$$

where F is the fused image.

The pseudo-code is in Algorithm 2.

6. **Experiments.** The proposed method based on the guided image filter (GIF) is compared with 5 different fusion algorithms based on contrast Laplacian pyramid (LAP) [7], shift-invariant wavelet transform (SIW) [8], image matting technique (IMT) [26], two-scale decomposition using the guided filter (TSD) [27] and multi-scale weighted gradient (MWG) [15] respectively.

The parameter settings of these methods are as follows. The default parameters given by the respective authors are adopted for the methods based on IMT, TSD and MWG. GIF: α is set to 0.2, the size of window of the majority filter l_1 and l_2 are set to 8 and 7 respectively, the radius of window r of the guided filter is set to 8, and ϵ of the guided filter is 0.03. LAP: 6 decomposition levels, the averaging scheme for the low frequency subband, the Li's choosing scheme [28] for the high frequency subband and the 9×9 window-based consistency check. SIW: 4 decomposition levels, the averaging scheme for the low frequency subband, the Li's scheme for the high frequency subband and the 3×3 window based consistency check.

Algorithm 2 The proposed image fusion method

function FUSION SCHEME(I^A, I^B)
  $M_p^A = (I^A * L)^2$
  $M_p^B = (I^B * L)^2$
  $M_b^A \leftarrow M_p^A$
  $M_b^B \leftarrow M_p^B$
  if $M_b^A > M_b^B$ **then**
    $D = 1$
  else
    $D = 0$
  end if
  D_b=MAJORITYFILTER(D, l_1)
  D_b=MAJORITYFILTER(D_b, l_2)
  $D_p = D_b \circledast W_8$
  D_2=GUIDEDFILTER(I^A, D_p)
  $F = D_2 I^A + (1 - D_2) I^B$
  return F
end function
function MAJORITYFILTER(D, l)
  $D = D - 0.5$
  $D = D * W_l$
  $D = D * W_l$
  if $D > 0$ **then**
    $D_b = 1$
  else
    $D_b = 0$
  end if
  return D_b
end function
function GUIDEDFILTER(I, p)
  Obtaining the q from I and p
  return q
end function

The fusion scheme is illustrated on four pairs of images: *Pepsi*, *Clock*, *Disk*, and *Lab*. Fig.4, Fig.5, Fig.6, and Fig.7 show the input images and the fusion results.

The performance metrics are depicted in the bar graphs Fig.8. The edge information based performance $Q_p^{ab|f}$ metric [31], structural similarity based metric $Q_w^{xy|f}$ [32] and phase congruency based metric Q_p [33, 34] are employed in evaluating the fusion quality.

Fig.10, Fig.11, Fig.12 and Fig.13 are cropped to show the fused result and the absolute value of the difference between the result and the focused reference part of image, and the peak signal-to-noise ratio (PSNR) between the result and the focused reference part of image is summarized in Table 1.

It can be seen that GIF and MWG obtains better visual effect and higher performance metrics than the others.

Fig.4(a)-(b) are two input images and Fig.4(c)-(h) are fusion results of different fusion schemes. Because of using high pass filter, there is the ringing effect in the fused results of LAP, SIW and TSD. The ringing effect can be seen from Fig.10. LAP, SIW, and TSD fuse the transform domain coefficients of both the input images other than selecting

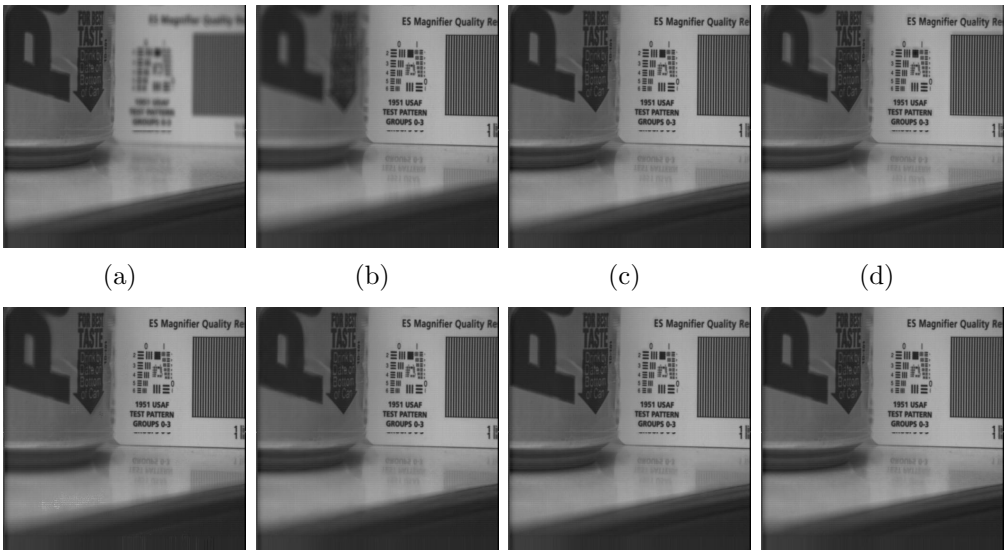

(a) (b) (c) (d)

(e) (f) (g) (h)

FIGURE 4. Input images and fused images obtained by different methods, (a) *Pepsi* 1, (b) *Pepsi* 2, (c) LAP, (d) SIW; (e) IMT, (f) TSD, (g) MWG, (h) GIF.

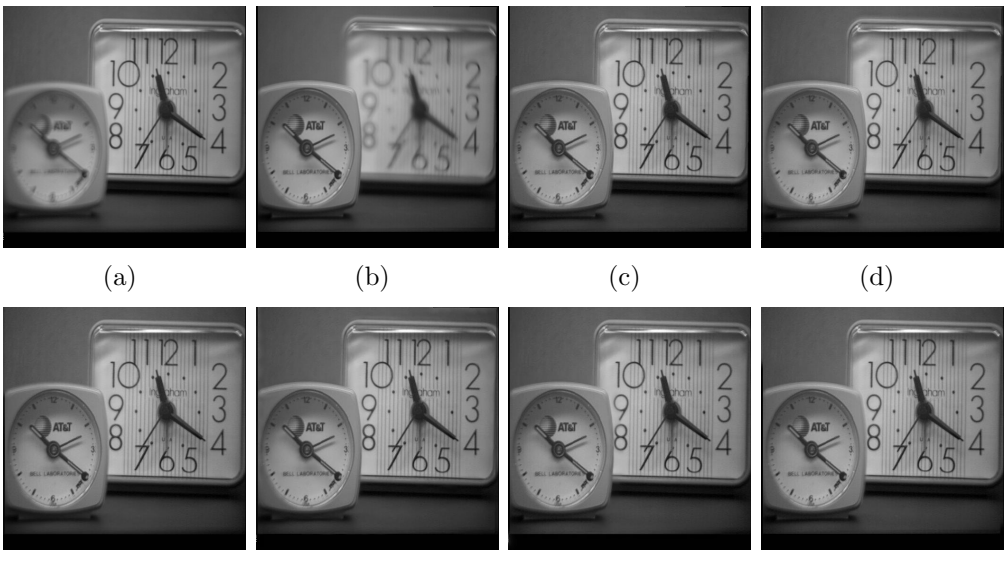

(a) (b) (c) (d)

(e) (f) (g) (h)

FIGURE 5. Input images and fused images obtained by different methods, (a) *Clock* 1, (b) *Clock* 2, (c) LAP, (d) SIW; (e) IMT, (f) TSD, (g) MWG, (h) GIF.

pixels either in I_A or in I_B, their results may be de-blurred the area where both the input images are blurred, and that may be added unpleasant effect in areas where one of the inputs has good clarity. There are a little shadows at the right up corner within the word 'ES Magnifier Quality' in Fig.4(c), Fig.4(d) and Fig.4(f), and it is most serious in SIW where not only the words zone but also the area below is shadow-surrounded. The shadows exist in LAP, SIW and TSD within the area around words zone. These results show that these fusion schemes tried to extract the focused content from both images but

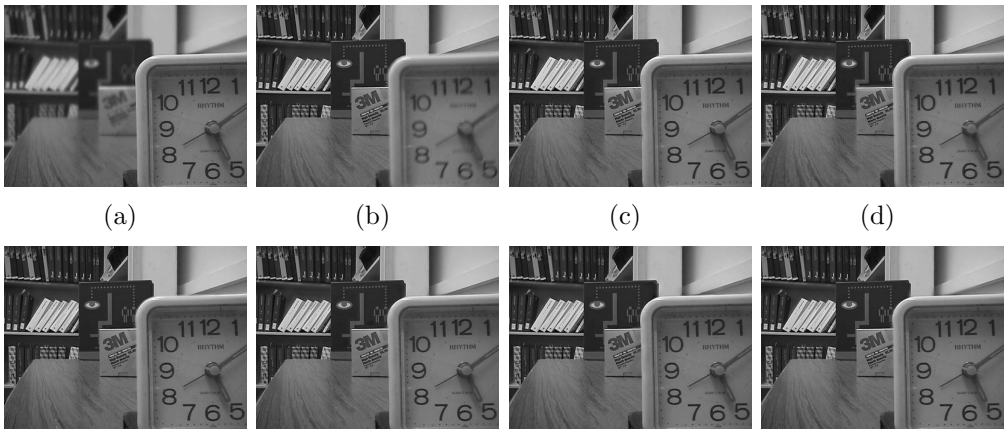

(a) (b) (c) (d)

(e) (f) (g) (h)

FIGURE 6. Input images and fused images obtained by different methods, (a) *Disk* 1, (b) *Disk* 2, (c) LAP, (d) SIW; (e) IMT, (f) TSD, (g) MWG, (h) GIF.

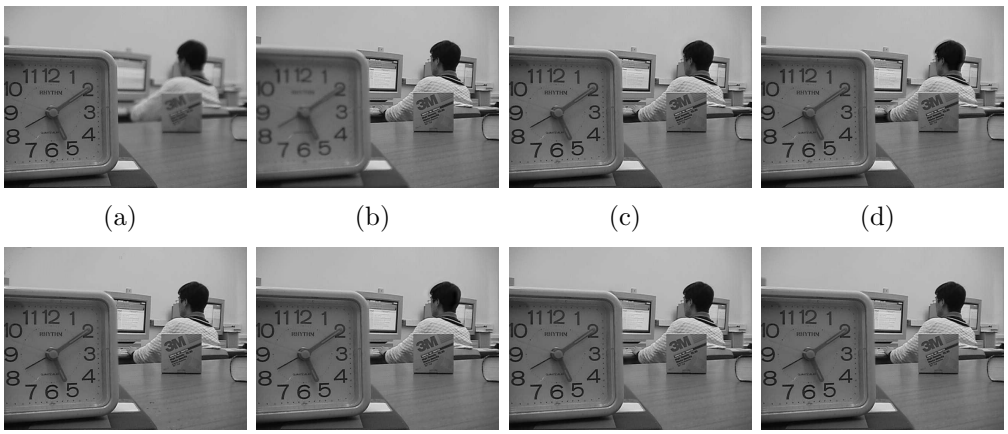

(a) (b) (c) (d)

(e) (f) (g) (h)

FIGURE 7. Input images and fused images obtained by different methods, (a) *Lab* 1, (b) *Lab* 2, (c) LAP, (d) SIW; (e) IMT, (f) TSD, (g) MWG, (h) GIF.

blurred areas have been left out to be shadows, and the shadows can also be seen as the blurred 'P' on the bottle and blurred at bottom of the bottle in Fig.4(e). Fig.4(e) has clear distortions of white spots in the left bottom around the border of the table as shown in Fig.9. The result of proposed scheme in Fig.4(h) avoids the shadow artifacts above and performs well. Fig. 10 shows the results of some compared areas. MWG and GIF method can preserve the features and details from the source images without producing visible artifacts. Because MWG has the processing of multi-scale decompositions and the calculating the eigenvalues, MWG has a high computational complexity.

As shown in Fig.5, Fig.11, Fig.6, and Fig.12, LAP, SIW and TSD has the ringing effect. As shown in Fig.9, there is a litter distorted in the image *Disk*. MWG and GIF obtain better visual effect than the others, and it can be seen at the bottom of left clock in the image *Clock*.

Returning to Fig.7 and Fig.13, method LAP creates a small alone around the head, SIW wrongs the arm, and TSD wrongs the head. Furthermore, IMT has some problems in the

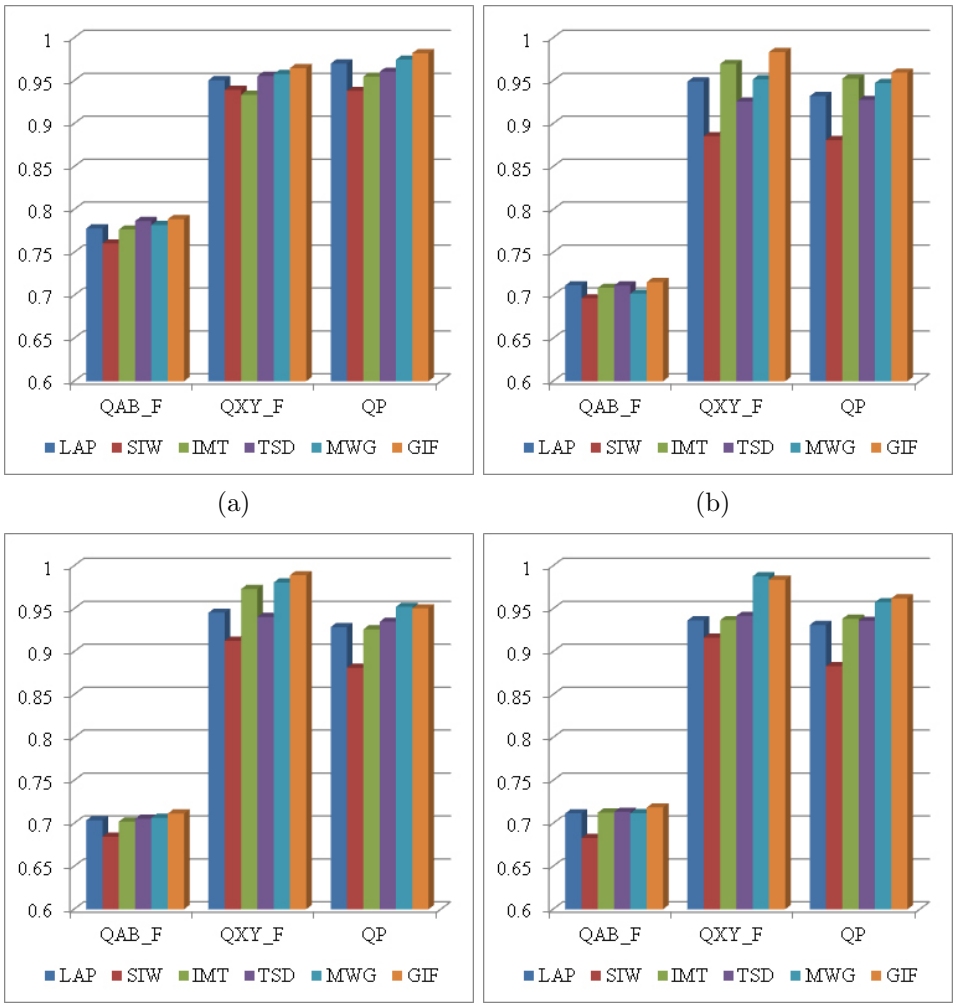

FIGURE 8. Quantitative evaluation, (a) *Pepsi*, (b) *Clock*; (c) *Disk*, (d) *Lab*.

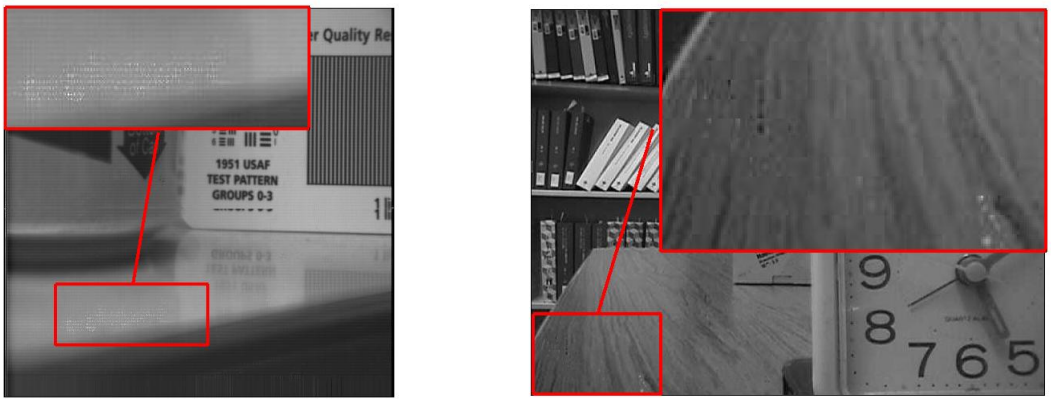

FIGURE 9. The fused result of IMT, (a) *Pepsi*, (b) *Disk*.

border area between clock and monitor. For these reasons, by using visual comparison, the best images result MWG and GIF. Therefore, this fact would confirm the numerical evidences reported in Fig. 8 and Table 1.

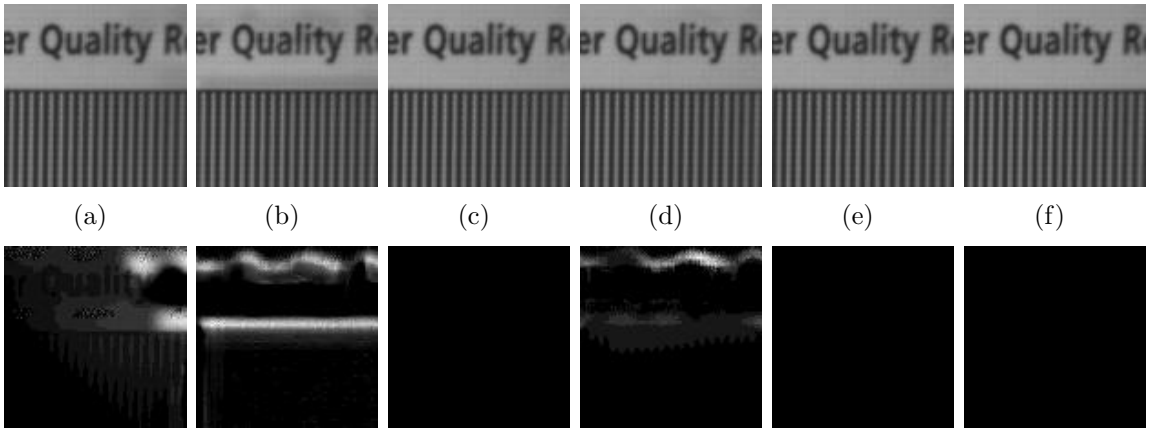

FIGURE 10. The fused results of the cropped part from the image *Pepsi*, (a) LAP, (b) SIW, (c) IMT, (d) TSD, (e) MWG, (f) GIF, and the absolute value of the difference between the result and the focused reference part of the image, (g) LAP, (h) SIW, (i) IMT, (j) TSD, (k) MWG, (l) GIF.

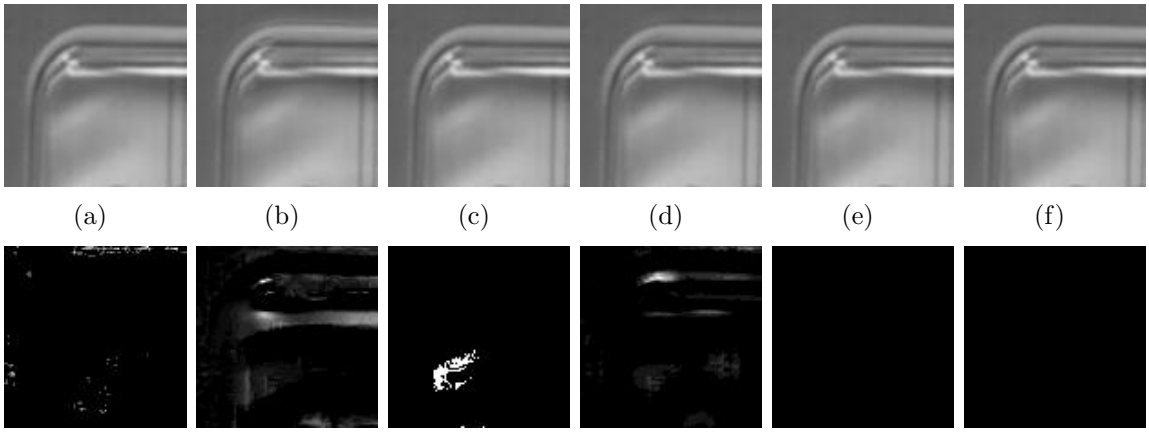

FIGURE 11. The fused results of the cropped part from the image *Clock*, (a) LAP, (b) SIW, (c) IMT, (d) TSD, (e) MWG, (f) GIF, and the absolute value of the difference between the result and the focused reference part of the image, (g) LAP, (h) SIW, (i) IMT, (j) TSD, (k) MWG, (l) GIF.

7. **Conclusion.** We use the energy of Laplacian to extract the local and sharp changes in intensity of images, and propose a new fusion method using guided image filter. the proposed multi-focus image fusion scheme outperforms the state of the art fusion methods, and it preserves well the detail information without producing artifacts and distortions.

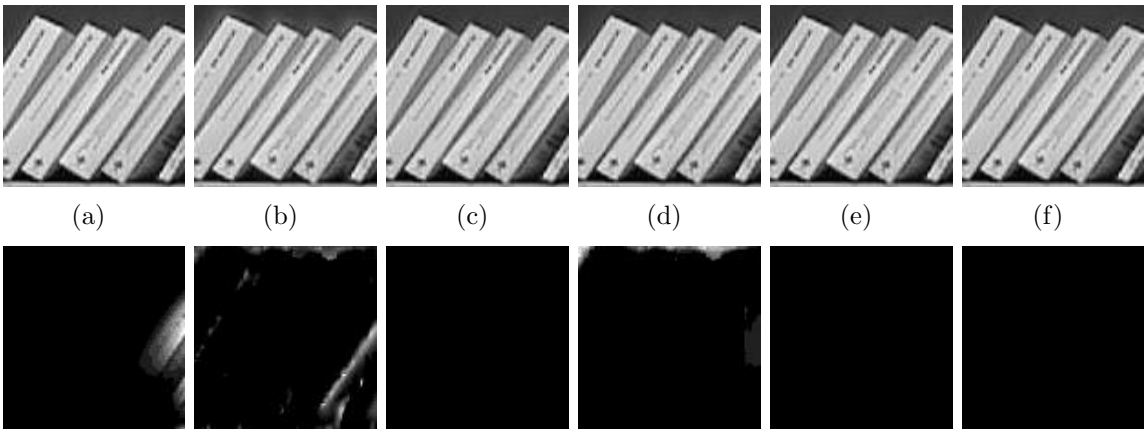

FIGURE 12. The fused results of the cropped part from the image *Disk*, (a) LAP, (b) SIW, (c) IMT, (d) TSD, (e) MWG, (f) GIF, and the absolute value of the difference between the result and the focused reference part of the image, (g) LAP, (h) SIW, (i) IMT, (j) TSD, (k) MWG, (l) GIF.

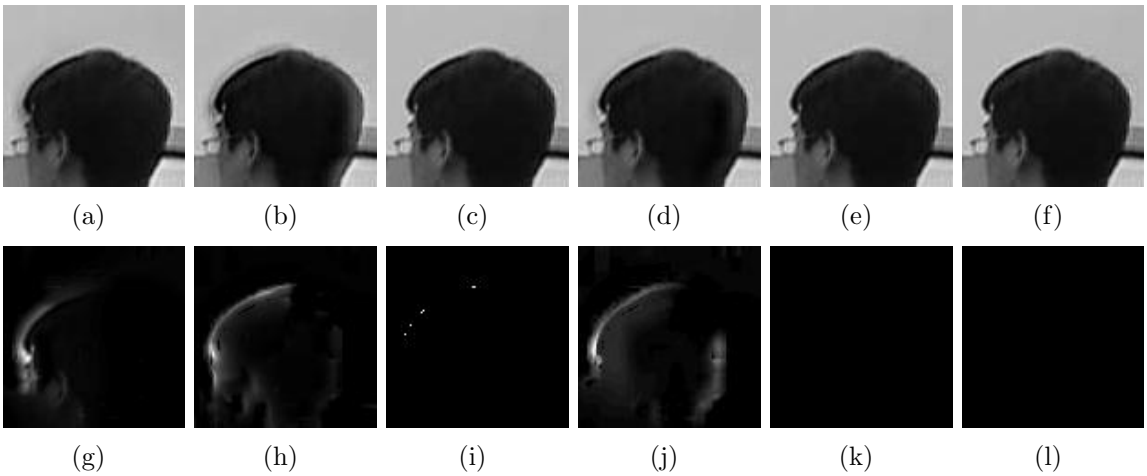

FIGURE 13. The fused results of the cropped part from the image *Lab*, (a) LAP, (b) SIW, (c) IMT, (d) TSD, (e) MWG, (f) GIF, and the absolute value of the difference between the result and the focused reference part of the image, (g) LAP, (h) SIW, (i) IMT, (j) TSD, (k) MWG, (l) GIF.

TABLE 1. Objective performance PSNR (dB)

	LAP	SIW	IMT	TSD	MWG	GIF
Pepsi	39.35	32.93	∞	45.90	∞	∞
Clock	48.71	34.18	60.82	43.26	∞	∞
Disk	34.38	31.35	∞	47.54	∞	∞
Lab	30.21	36.86	80.35	34.19	∞	∞

Acknowledgment. This work has been supported by the National Science Foundation of China under the Grant No. 61201422, the Specialized Research Fund for the Doctoral Program of Higher Education under the Grant No. 20120211120013, and the Fundamental Research Funds for the Central Universities under the Grant No. lzujbky-2013-38.

REFERENCES

[1] S. Cheng, H. Chooi, Q. Wu and K. Castleman, Extended depth-of-field microscope imaging: Mpp image fusion vs. wavefront coding, in: *IEEE International Conference on Image Processing*, pp. 2533-2536, 2006.

[2] R. Martinez-Cuenca, G. Saavedra, M. Martinez-Corral and B. Javidi, Extended depth-of-field 3-d display and visualization by combination of amplitude-modulated microlenses and deconvolution tools, *Journal of Display Technology*, vol. 1, no. 2, pp. 321-327, 2005.

[3] O. Cossairt, C. Zhou, and S. Nayar, Diffusion coded photography for extended depth of field, *ACM Trans. on Graphics*, vol. 29, no. 4, pp. 31, 2010.

[4] O. Cossairt, M. Gupta and S. K. Nayar, When does computational imaging improve performance, *IEEE Trans. on Image Processing*, vol. 22, no. 2, pp. 447-458, 2013.

[5] Y. Bando, H. Holtzman and R. Raskar, Near-invariant blur for depth and 2d motion via time-varying light field analysis, *ACM Trans. on Graphics*, vol. 32, no. 2, pp. 13, 2013.

[6] P. J. Burt and E. H. Adelson, Merging images through pattern decomposition, *Applications of Digital Image Processing VIII*, vol. 575, pp. 173-181, 1985.

[7] A. Toet, L. J. Van Ruyven and J. M. Valeton, Merging thermal and visual images by a contrast pyramid, *Optical Engineering*, vol. 28, no. 7, pp. 2877-2877, 1989.

[8] O. Rockinger, Image sequence fusion using a shift-invariant wavelet transform, *IEEE International Conference on Image Processing*, vol. 3, pp. 288-291, 1997.

[9] Z. Zhang and R. S. Blum, A categorization of multiscale-decomposition-based image fusion schemes with a performance study for a digital camera application, *Proc. of the IEEE*, vol. 87, no. 8, pp. 1315-1326, 1999.

[10] G. Piella, A general framework for multiresolution image fusion: from pixels to regions, *Information Fusion*, vol. 4, no. 4, pp. 259-280, 2003.

[11] G. Pajares and J. Manuel de la Cruz, A wavelet-based image fusion tutorial, *Pattern recognition*, vol. 37, no. 9, pp. 1855-1872, 2004.

[12] S. Li, B. Yang and J. Hu, Performance comparison of different multi-resolution transforms for image fusion, *Information Fusion*, vol. 12, no. 2, pp. 74-84, 2011.

[13] R. Redondo, F. Šroubek, S. Fischer, and G. Cristóbal, Multifocus image fusion using the log-gabor transform and a multisize windows technique, *Information Fusion*, vol. 10, no. 2, pp. 163-171, 2009.

[14] T. Li and Y. Wang, Biological image fusion using a nsct based variable-weight method, *Information Fusion*, vol. 12, no. 2, pp. 85-92, 2011.

[15] Z. Zhou, S. Li and B. Wang, Multi-scale weighted gradient-based fusion for multi-focus image, *Information Fusion*, vol. 20, pp. 60-72, 2014.

[16] M. Subbarao and J. K. Tyan, Selecting the optimal focus measure for autofocusing and depth-from-focus, *IEEE Trans. on Pattern Analysis and Machine Intelligence*, vol. 20, no. 8, pp. 864-870, 1993.

[17] W. Huang and Z. Jing, Evaluation of focus measures in multi-focus image fusion, *Pattern Recognition Letters*, vol. 28, no. 4, pp. 493-500, 2007.

[18] H. Zhao, Z. Shang, Y. Y. Tang and B. Fang, Multi-focus image fusion based on the neighbor distance, *Pattern Recognition*, vol. 46, no. 3, pp. 1002-1011, 2013.

[19] S. Li, J. T. Kwok and Y. Wang, Multifocus image fusion using artificial neural networks, *Pattern Recognition Letters*, vol. 23, no. 8, pp. 985-997, 2002.

[20] H. A. Eltoukhy and S. Kavusi, Computationally efficient algorithm for multifocus image reconstruction, *Electronic Imaging*, pp. 332–341, 2003.

[21] X. Zhang, X. Li, Z. Liu and Y. Feng, Multi-focus image fusion using image-partition-based focus detection, *Signal Processing*, vol. 102, pp. 64-76, 2014.

[22] S. Li, J. T. Kwok and YY. Wang, Combination of images with diverse focuses using the spatial frequency, *Information Fusion*, vol. 2, no. 3, pp.169-176, 2001.

[23] S. Li, J. Y. Kwok, I. W. Tsang and Y.Y. Wang, Fusing images with different focuses using support vector machines, *IEEE Trans. on Neural Networks*, vol. 15, no. 6, pp. 1555-1561, 2004.

[24] W. Huang and Z. L. Jing, Multi-focus image fusion using pulse coupled neural network, *Pattern Recognition Letters*, vol. 28, no. 9, pp. 1123-1132, 2007.

[25] D. Agrawal and J. Singhai, Multifocus image fusion using modified pulse coupled neural network for improved image quality, *IET Image Processing*, vol. 4, no. 6, pp.443-451, 2010.

[26] S. Li, X. Kang, J. Hu and Y.B.. Yang, Image matting for fusion of multi-focus images in dynamic scenes, *Information Fusion*, vol. 14, no. 2, pp. 147-162, 2013.

[27] S. Li, X. Kang and Y.J. Hu, Image fusion with guided filtering, *IEEE Trans. on Image Processing*, vol. 22, no. 7, pp. 2864-2875, 2013.
[28] H. Li, B. S. Manjunath and S. K. Mitra, Multisensor image fusion using the wavelet transform, *Graphical models and image processing*, vol. 57, no. 3, pp.235-245, 1995.
[29] K. He, J. Sun and YX. Tang, Guided image filtering, *IEEE Trans. on Pattern Analysis and Machine Intelligence*, vol. 35, no. 6, pp. 1397-1409, 2013.
[30] N. R. Draper and Y.H.Smith, *Applied regression analysis 2nd ed*, 1981.
[31] C.S. Xydeas and V. Petrović, Objective image fusion performance measure, *Electronics Letters*, vol. 36, no. 4, pp. 308-309, 2000.
[32] C. Yang, J. Q. Zhang, X. R. Wang and Y. X. Liu, A novel similarity based quality metric for image fusion, *Information Fusion*, vol. 9, no. 2, pp.156-160, 2008.
[33] J. Zhao, R. Laganiere and Y. Z. Liu, Performance assessment of combinative pixel-level image fusion based on an absolute feature measurement, *International Journal of Innovative Computing, Information and Control*, vol. 3, no. 6, pp. 1433-1447, 2007.
[34] Z. Liu, D. S. Forsyth and Y. R. Laganière, A feature-based metric for the quantitative evaluation of pixel-level image fusion, *Computer Vision and Image Understanding*, vol. 109, no. 1, pp.56-68, 2008.